Surface Science 603 (2009) 2574–2579

Contents lists available at ScienceDirect

Surface Science

journal homepage: www.elsevier.com/locate/susc

The Fe_3O_4 origin of the "Biphase" reconstruction on α-Fe_2O_3(0 0 0 1)

Courtney H. Lanier [a,b], Ann N. Chiaramonti [a,b], Laurence D. Marks [a,b,*], Kenneth R. Poeppelmeier [b,c]

[a] Department of Materials Science and Engineering, Northwestern University, Evanston, IL, USA
[b] Institute for Catalysis in Energy Processes, Northwestern University, Evanston, IL, USA
[c] Department of Chemistry, Northwestern University, Evanston, IL, USA

ARTICLE INFO

Article history:
Received 10 April 2009
Accepted for publication 8 June 2009
Available online 13 June 2009

Keywords:
Electron microscopy
Surface structure
Iron oxide

ABSTRACT

The so-called Biphase termination on α-Fe_2O_3 has been widely accepted to be a structure with a ~40 Å unit supercell composed of coexisting islands of $Fe_{1-x}O$ and α-Fe_2O_3. Based on thermodynamic arguments and experimental evidence, including transmission electron diffraction, imaging, magnetic and spectroscopic information, it is found that the previously proposed structure model is inaccurate. The actual Biphase structure is instead a layered structure related to the reduction of α-Fe_2O_3 to Fe_3O_4. A model for the Biphase termination is proposed which does not contain islands of $Fe_{1-x}O$ but instead consists of bulk α-Fe_2O_3 and a Fe_3O_4-derived overlayer. The proposed model is consistent with all current and previously reported experimental findings.

1. Introduction

α-Fe_2O_3 and its surface structure are of great interest in fields such as catalysis, geochemistry, water purification, and magnetic recording media. Of all the dehydrated iron oxides, α-Fe_2O_3 is the most prevalent in soils and sediments, playing a role in many geochemical cycles [1,2]. α-Fe_2O_3 has been investigated as a catalyst for the removal/decomposition of soil and air pollutants, including 2-chlorophenol [3], aminophenol [4], and SO_2 [5,6]. α-Fe_2O_3 is also active for the dehydrogenation of ethylbenzene to styrene [7], and although low, the activity is enhanced by the addition of alkali [8]. α-Fe_2O_3 has the corundum structure, with $a = 5.035$ Å and $c = 13.749$ Å. Iron cations, in the oxidation state Fe^{3+}, occupy slightly distorted oxygen octahedra in two-thirds of the possible octahedral sites of the hexagonally close packed oxygen framework. Along the [0 0 1] direction the layer stacking is –(O_3–Fe)–(Fe–O_3)– so the (cleavage) valence charge neutral surface is terminated by either 3 oxygen atoms or 1 iron atom per 5.035 Å × 5.035 Å 1 × 1 surface unit cell. The (0 0 0 1) basal plane is a naturally-occurring surface in mineralogical specimens and is the focus of this work.

The (0 0 0 1) surface of α-Fe_2O_3 has been studied extensively, however the results [9–22] are often contradictory. For example, several groups have observed the presence of hexagonally symmetric satellite spots surrounding the {1 1 0}-type spots in a LEED pattern of the (0 0 0 1) surface following annealing treatment in vacuum. The interpretation of such a LEED pattern is not straightforward, and several structure models for its origin have been proposed of which there are two main competing arguments. The first is that the hexagonally symmetric satellite spots have their origin in multiple-scattering across an interface, and the second posits that the satellite spots are due to coexisting islands of mesoscopic dimension, and do not come from a layered structure.

First to report such satellite spots and propose a structure model for their origin were Lad and Henrich [9], who observed a LEED pattern with six-fold symmetric satellite spots following annealing at 900 °C for 30 min in 1×10^{-6} Torr O_2. Annealing at 1×10^{-10} Torr O_2 produced the same LEED pattern coexisting with that of a Fe_3O_4(1 1 1) surface termination. The hexagonally symmetric satellite spots were attributed to multiple-scattering across an interface, and while an Fe_3O_4(1 1 1)/α-Fe_2O_3(0 0 0 1) interface was first considered, diffraction from an $Fe_{1-x}O$(1 1 1)/α-Fe_2O_3(0 0 0 1) interface (as envisaged from a simple multiple-scattering model) more closely approximated their data. Thus a $Fe_{1-x}O$(1 1 1)/α-Fe_2O_3(0 0 0 1) interface was assumed. Barbieri et al. [10] reported a Fe_3O_4-type overlayer on a germanium-doped chemical vapor deposition grown (CVT) (0 0 0 1) α-Fe_2O_3 crystal annealed at 627 °C in 1×10^{-10} and 1×10^{-6} Torr O_2. Subsequent treatment at 727 °C caused a change in the structure of the overlayer, and the authors assumed it to be the formation of α-Fe_2O_3 although the formation of an ordered array of oxygen-defects could not be ruled out. Further annealing at 927 °C generated a LEED pattern with hexagonally symmetric satellite spots, and the authors attributed the pattern to the formation of a $Fe_{1-x}O$ overlayer on top of the α-Fe_2O_3 layer based on the observation of a 3.0 Å unit cell. Diffraction spots from Fe_3O_4 were still present, and thus the proposed α-Fe_2O_3/$Fe_{1-x}O$ layer was in coexistence with the Fe_3O_4 layer. Further supporting the idea that satellite spots are related

* Corresponding author. Address: Department of Materials Science and Engineering, Northwestern University, 2220 N Campus Drive, Evanston, IL 60201, USA.
E-mail address: L-marks@northwestern.edu (L.D. Marks).

0039-6028/$ - see front matter © 2009 Elsevier B.V. All rights reserved.
doi:10.1016/j.susc.2009.06.006

to scattering across an interface between Fe_2O_3 and its reduction products is the study by Kim et al. [22]. There it was found that the surface of a post-sputtered sample was non-stoichiometric, but upon annealing at low temperatures and high oxygen pressure the outer-most surface recovered to α-Fe_2O_3 while a sub-surface region remained as remnant Fe_3O_4. In effect, the outer α-Fe_2O_3 acted as a barrier for propagation of the oxidation front to the Fe_3O_4 remnant below. The authors proposed that the remnant Fe_3O_4 sub-surface phase could be regarded as a defect layer in the α-Fe_2O_3 crystal, and that full reoxidation of the crystal required segregation of the reduced defect layer to the outer-most surface. As soon as the sample was heated to 745 °C, a LEED pattern with hexagonally symmetric satellite spots was observed, which the authors interpreted to be the structure that exists once the defect phase (presumably related to Fe_3O_4) has segregated to the top surface.

Differing from the previous studies, Condon et al. [11] attributed the hexagonally symmetric satellite spots observed in their LEED pattern following annealing at 800 °C in 7.75×10^{-7} Torr O_2 to the coexistence of α-Fe_2O_3 and $Fe_{1-x}O$ phases on the surface of α-Fe_2O_3. This interpretation was based on the corrugation spacing observed by STM. Specifically, domains of 5 Å and 3 Å periodicity were attributed to α-Fe_2O_3 and $Fe_{1-x}O$, respectively. These were arranged in a 40 ± 5 Å superlattice cell rotated 30° relative to the α-Fe_2O_3 1×1. The authors coined the term "Biphase ordering" to describe that structure and proposed a model for its formation, suggesting a close packed layer of oxygen with $Fe_{1-x}O$ spacing nucleated on the surface of α-Fe_2O_3. Iron cations were then incorporated, with some minor adjustments of the oxygen lattice, to form domains of α-Fe_2O_3 and domains of $Fe_{1-x}O$. Although this model required the growth of a layer, the authors emphasized that the Biphase surface was comprised of "islands of mesoscopic dimensions" and is not a layered structure. No mention was made of the oxidation state of the iron cations, and thus it is unknown how the surface would achieve valence charge neutrality for this proposed structure.

Since the publication of the α-Fe_2O_3/$Fe_{1-x}O$ coexisting island structure model by Condon et al., the Biphase termination has been the predominant model for the actual structure of the surface in the surface science community and is often assumed whenever a LEED pattern with hexagonally symmetric satellite spots is observed on α-Fe_2O_3(0 0 0 1) following annealing in vacuum [15,17–19,21]. The idea of multiple-scattering from an interface related to the reduction of Fe_2O_3 has largely been ignored. In this paper, we present evidence from an examination of high energy electron diffraction data, analysis of the redox thermodynamics for the Fe–O system, magnetism measurements and spectroscopic examination of similarly prepared surfaces that the hexagonally symmetric satellite spots have their origin in a simple Fe_3O_4 on Fe_2O_3 overlayer.

Through an analysis of the previous reports, summarized in Table 1, it becomes clear that the interpretation of six-fold satellite spots in the LEED pattern of annealed α-Fe_2O_3 is open to question. First, in almost all cases the annealing is in 10^{-6} to 10^{-7} Torr of oxygen for temperatures ranging from 550 to 957 °C. As will be discussed in more detail later, if the sample is in equilibrium with the gas phase oxygen under such conditions bulk Fe_3O_4 is the stable phase and a far more reducing atmosphere of 10^{-12} to 10^{-15} Torr of oxygen is needed to produce FeO in the bulk, see Fig. 1. (Details of how the phase diagram was calculated are given later.) Second, in several of the cases the structure was observed on oxidation of Fe_3O_4.

As in most oxides, oxygen is preferentially sputtered from α-Fe_2O_3 when Ar^+ ion-milled, and the ion milling-induced reduction of pure α-Fe_2O_3 is well-known [23–25]. Upon heat treatment, the presence of a reduced layer at the surface of α-Fe_2O_3 could act as a nucleation site for the growth of Fe_3O_4 at the surface, and further, serve to lower the activation barrier for the propagation of Fe_3O_4 domains into the bulk of the material. The reducing effects of ion milling are enhanced by the presence of contaminants in the α-Fe_2O_3 crystal. Not only does the surface preferentially lose oxygen, a spinel phase can form on the near-surface region of impure α-Fe_2O_3 after Ar^+ ion bombardment [26] with no heat treatment required. In fact, impurity levels as low as 0.2 at.% have been shown to stabilize the formation of the spinel phase. This impurity level is just at the 0.1–0.5 at.% detection limit of Auger electron spectroscopy (AES), which is commonly used in conjunction with LEED. Because the spinel structure is not exactly coincident with the underlying Fe_2O_3 one easily obtains a "floreted" diffraction pattern by simple double-diffraction. Unlike contamination-induced spinel phases which arise from lower concentrations of impurities, this particular spinel phase – and thus the floreted diffraction pattern – persisted even after annealing.

In nearly two-thirds of the reported cases, the Biphase termination is observed on contaminant-containing samples, either natural minerals [9,11,15,19,22,27] or doped CVT crystals [10] that have been Ar^+ sputtered prior to annealing. As nearly all mineralogical samples contain impurities (in the case of the doped CVT

Table 1
Summary of previous reports and details of the Biphase termination on α-Fe_2O_3.

Structure	Temperature (°C)	Pressure (Torr)	Time (min)	Sample type	Method	References
FeO/Fe_2O_3	677	1.0×10^{-6}	N/A	Fe_3O_4	STM	Berdunov et al. [50]
Fe_3O_4	N/A	N/A	N/A	Oxidized Fe_3O_4	N/A	Huang et al. [29]
Biphase	550	7.5×10^{-6}	120	Thin film on Pt(1 1 1)	LEED	Leist et al. [21]
Biphase	612	UHV	30	Mineralogical	LEED	Herman et al. [15]
Biphase	627	7.5×10^{-7}	N/A	Thin film on Pt(1 1 1)	LEED	Huang et al. [29]
Biphase	773	3.75×10^{-5}	30	Mineralogical	STM, LEED	Ketteler et al. [18]
Biphase	745	2×10^{-5}	30	Mineralogical oxidized Fe_3O_4	X-ray scattering, LEED	Kim et al. [22]
Biphase	800	7.5×10^{-7}	N/A	Mineralogical	STM, LEED	Condon et al. [11]
Biphase	800	7.5×10^{-7}	N/A	Thin film on Pt(1 1 1)	STM, LEED	Shaikhutdinov and Weiss [17]
Biphase	900	1×10^{-6}	30	Mineralogical	LEED, XPS	Lad and Henrich [9]
Biphase and Fe_3O_4	900	1×10^{-10}	N/A	Mineralogical	STM, LEED	Lad and Henrich [9]
Biphase and Fe_3O_4	927	1×10^{-6}	5	CVT, germanium-doped, Fe_3O_4 overlayer	LEED, XPS	Barbieri et al. [10]
Biphase and Fe_3O_4	927	1×10^{-6}	5	Mineralogical	LEED, XPS	Barbieri et al. [10]
Biphase and Fe_3O_4	927	UHV	N/A	Mineralogical	LEED	Camillone et al. [19]
Biphase	957	5×10^{-5}	2	Mineralogical	LEED	Camillone et al. [19]
Biphase	957	UHV	15	Mineralogical	LEED	Camillone et al. [19]

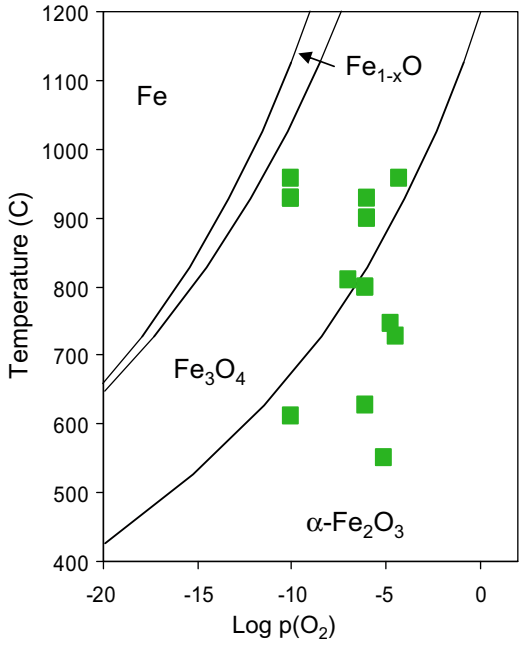

Fig. 1. Phase diagram for the iron–oxygen system calculated from Ref. [46]. Marked on the phase diagram are the conditions previously reported for the formation of the Biphase structure on α-Fe_2O_3.

crystal, Ge was intentionally present at levels up to 0.02 at.%), and ion milling was always employed to prepare the Biphase samples, one must keep in mind the implications of the impurity-stabilized near-surface spinel phase on the interpretation of the Biphase surface.

For the remaining studies listed in Table 1, the iron oxide specimens were grown as thin films on Pt(1 1 1) with thicknesses reported to be several ML (monolayers) up to 50 nm [17,21,28,29] and the films were not sputtered prior to annealing. In these studies the Pt substrate was assumed to have no role in the structural dynamics of the iron oxide film. However, the effects of the Pt substrate cannot be ignored based on work by Nahm et al. [30] Liu et al. [31] and Dieckmann [32,33]. Nahm et al. observed the formation of $FePt_3$ ordered alloys due to interdiffusion of ultrathin Fe films with a Pt substrate upon annealing, and Liu et al. observed PtFe ordered alloys existing in equilibrium with α-Fe_2O_3 and/or Fe_3O_4. Finally, Dieckmann et al. found that Pt crucibles used to anneal Fe_3O_4 changed the stoichiometry of the iron oxide. Thus the use of Pt substrates could influence the structure.

2. Experimental method

Two different types of raw-material samples were used in this work. The first were mineralogical samples obtained from naturally-occurring high-purity "iron rosette" crystals (Brazil), and the second were pure single crystals grown in an optical image furnace [34]. Because upon ion milling impure crystals (e.g. mineralogical in origin) can form a spinel phase near the surface which does not form with the very pure single crystals, the later serve as an important check against impurity dependent artifacts. No difference was observed in the behavior of the two types of samples, so this can be ruled out.

Transmission electron microscopy specimens were made from oriented single crystals cut into 3 mm disks using a rotary disc cutter, thinned by hand to ~100 μm using fine grit silicon carbide sandpaper, and dimpled such that the center part of the disk was >15 μm and the outer rim of the sample remained at ~100 μm. The samples were milled with 3.8–5 keV Ar^+ ions for approximately 2–5 h until electron transparent.

Owing to the possibility of the near-surface spinel phase [26], samples were subjected to a pre-treatment anneal in flowing O_2 for 0.5–2 h at 850 °C to remove the spinel phase (if present), repair damage imparted to the specimen upon preparation, and obtain a 1×1 surface reconstruction of α-Fe_2O_3. These samples were transferred to a UHV-electron microscope (base pressure 1×10^{-10} Torr) with an attached UHV side chamber (SPEAR). Mimicking the traditional surface science preparation regimes, the samples were cyclically milled with 1 keV Ar^+ ions at ~60° from the surface normal for approximately 5 min on each side, then annealed with a low-voltage electron gun in pressures ranging from UHV to 1×10^{-6} Torr O_2; the temperatures of the samples measured with an optical pyrometer. X-ray photoelectron spectroscopy (XPS) spectra were acquired before and after each Ar^+ ion milling or annealing treatment and were used to check for the presence of carbon and qualitatively monitor the oxidation state of the iron.

Transmission electron microscopy was performed in the attached Hitachi UHV-H9000 operated at 300 keV; information on using transmission electron microscopy to study surfaces has been given elsewhere [35–40]. An in situ test for the presence of magnetism in the single crystal TEM specimens, as a way to empirically identify possible phases, was developed based on the attraction of unfixed specimens to the strong magnetic field of the objective lens of the microscope. In most modern conventional TEMs, the objective lens is an electromagnetic immersion lens split into an upper and lower pole. In normal operation, the specimen sits in the gap between the two poles, rigidly fixed inside of a stage or holder. Due to the unique design parameters and sample loading procedures of the UHV microscope, the objective lens pole gap can be viewed easily through a UHV compatible window in the side of the microscope and specimens can be brought near to the pole pieces while not rigidly affixed to the specimen stage. By slowly and carefully moving an unconstrained TEM sample near to the lens gap (with the lens current on), a movement or attraction of the sample to the lens, if observed, indicates the presence of a ferrimagnetic or ferromagnetic phase in the specimen. Since the specimens were all subject to a reducing anneal, the possibility that the apparent magnetism results from the presence of ferrimagnetic γ-Fe_2O_3 (where all the iron is fully oxidized in the 3+ state) can be ruled out. The presence of a nonequilibrium amorphous ferrimagnetic phase can be ruled out given the fact that diffraction spots corresponding to a known crystal structure were always observed. Ferromagnetic iron can be ruled out because iron was never observed to be present in the 0+ oxidation state as verified by XPS. α-Fe_2O_3 is antiferromagnetic and was never observed to be attracted to the magnetic pole piece. Similarly, FeO is antiferromagnetic and not expected to interact with the magnetic field. Therefore, an attraction to the magnetic field of the pole piece in the electron microscope is indicative of the presence of ferrimagnetic Fe_3O_4 or a related crystalline phase in the TEM specimen.

3. Results

We initially attempted to reproduce the Biphase surface by copying the conditions reported in the literature with sputter-cleaning/annealing cycles. In nearly 30 experiments, the characteristic floreted diffraction pattern was never observed although the specimens were often observed to be attracted to the magnetic field of the pole piece, indicating ferrimagnetism. For reference, further background details as well as diffraction data not included here can be found in the PhD theses of Chiaramonti [41] and Lanier [42]. More useful was a systematic search, performed by annealing in different pressures of O_2, the results of which are summarized in Table 2.

Table 2
Results for a systematic search for the Biphase surface: temperature, pressure, and observed bulk phase.

Temperature (°C)	Pressure (Torr O_2)	Time (min)	Observed phase
650	5×10^{-7}	20	Fe_3O_4
700	5×10^{-7}	20	α-Fe_2O_3
750	5×10^{-7}	20	α-Fe_2O_3
800	1×10^{-6}	20	α-Fe_2O_3
810	1.1×10^{-7}	20	Biphase
850	1×10^{-6}	15	Fe_3O_4*

* Possibly a phase mixture of Fe_3O_4 and α-Fe_2O_3.

At low temperatures (650 °C), Fe_3O_4 was present on the surface of α-Fe_2O_3 owing to insufficient diffusion (for this time and temperature) to drive the recovery of the surface from the ion-milled or reduced state. At higher temperatures (700–800 °C), the 1×1 surface of α-Fe_2O_3 was formed. TEM images showed that the surface was starting to facet and diffraction patterns showed streaking, which indicates that the surface was evolving towards a flat, equilibrium structure.

A sample annealed for 20 min in 1.1×10^{-7} Torr O_2 at 810 °C did form a "floreted" diffraction pattern (shown in Fig. 2), the nominal fingerprint of the Biphase, however these conditions were not exactly the same as those reported in the literature.

At 850 °C, the sample transformed (in part or entirely) to Fe_3O_4 or another ferrimagnetic cubic spinel phase, as evidenced by an extremely strong attraction of the sample to the magnetic pole piece of the TEM.

Focusing on Fig. 2, the intensity of the floret was not uniform as there were two bright spots per floret shown with arrows. Note that the distance between the paired bright spots increases with increasing distance from the center of the pattern. In LEED diffraction is dynamical and it can be tricky to differentiate between spots present due to double-diffraction and those due to a superstructure. With TEM this is far easier, because a near kinematical

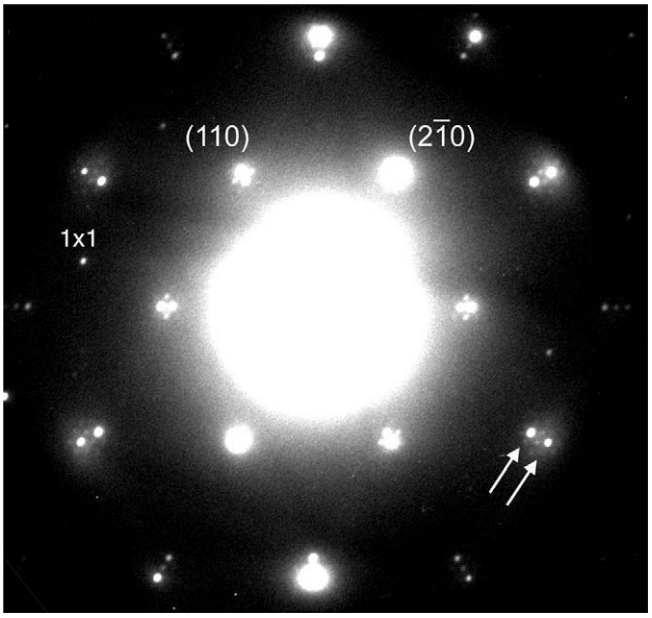

Fig. 2. Off-zone transmission electron diffraction pattern from a α-Fe_2O_3 TEM sample annealed in 1.1×10^{-7} Torr O_2 at 810 °C for 20 min exhibiting a floreted pattern. Strong diffraction indicating hex-on-hex epitaxy is observed (arrowed). Relatively weak spots at the locations of the 1×1 surface lattice are present, one of which is marked; these should rigorously be interpreted as higher-order Laue zone reflections.

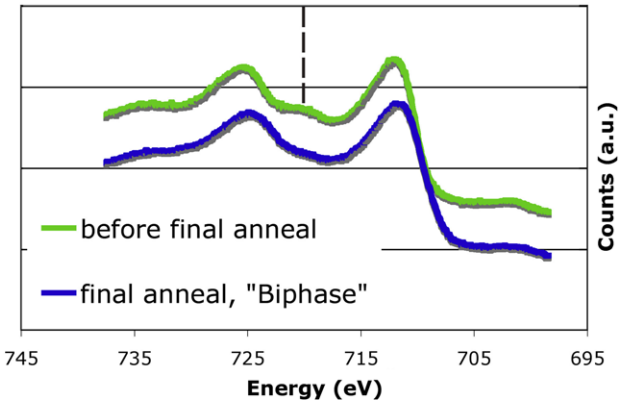

Fig. 3. X-ray photoelectron spectra of the surface of α-Fe_2O_3 before and after the annealing. The Fe^{3+} satellite peak (marked with dashed line) is observed before the anneal, but is lower in intensity after the anneal, indicating reduction to Fe^{2+}.

diffraction condition can easily be reached by simply tilting the specimen away from the zone axis. Fig. 2 is a text-book example of double-diffraction from two epitaxial crystals [43], here hex-on-hex epitaxy. Diffraction from the crystalline overlayer (the inner spots in Fig. 2) indicates that the structure is simple, as it has a simple hexagonal pattern with weak intensity modulations.

A brief explanation is appropriate to emphasize the difference between what LEED, STM and TED show in problems like this. As is well-known, LEED involves scattering primarily from the atomic core potential, but is strongly dynamical so one can rarely say whether satellite spots (e.g. the floret spots) are reciprocal lattice vectors with appreciable structure-factors, or very weak structure factor reflections appearing due to dynamical diffraction. As is also well-known, STM only shows the joint density-of-states, not the atomic sites; sometimes they are similar, but often they are not. Done correctly with an off-zone tilt, TED from a surface is >95% kinematical so we can unconditionally state that the floret spots are due to dynamical diffraction. Omitting these spots, all one has is a simple hexagonal surface structure which can be inverted to the potential almost by hand (e.g. [44]), although this would not add more information so is not included here. The "Biphase" structure with domains of 5 Å and 3 Å periodicity due to both α-Fe_2O_3 and $Fe_{1-x}O$ would have a much more complicated diffraction pattern and can be unconditionally ruled out.

X-ray photoelectron spectroscopy was performed on this α-Fe_2O_3 sample before and after the formation of the floreted diffraction pattern and the results are shown in Fig. 3. Prior to annealing the Fe^{3+} satellite peak (marked with a dashed line in the figure) at ~719.8 eV is present, as expected for clean α-Fe_2O_3. After the anneal, the Biphase surface shows a significant decrease in intensity of the Fe^{3+} satellite peak, indicative of reduction and Fe^{2+} formation [45].

4. Model for the Biphase

In this section a model is proposed for the Biphase structure based upon both consideration of the bulk thermodynamics as well as the diffraction, XPS and the magnetization tests described above.

The Fe–O bulk phase diagram, shown in Figs. 1 and 4, was calculated from thermodynamic free energy data [46], and is similar to those presented by Muan [47], Miser et al. [48], and Ketteler et al. [18]. The pressure is plotted as $\log(pO_2)$ (Torr) and temperature in degrees celsius, such that the lower right corner of the diagram is nominally oxidized relative to the upper left corner. In general, increasing temperature or decreasing pressure results in

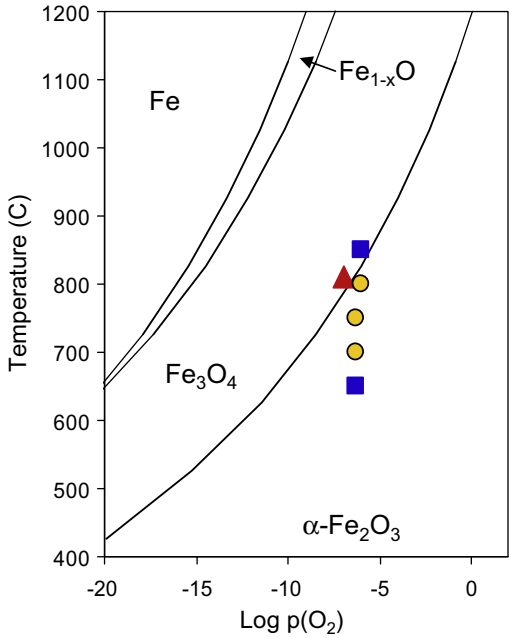

Fig. 4. Phase diagram for the iron–oxygen system calculated from Ref. [46]. Marked on the phase diagram are the conditions where Fe_3O_4 was observed (blue squares), Fe_2O_3 (yellow circles) and the Biphase diffraction pattern (red triangle). (For interpretation of the references to colour in this figure legend, the reader is referred to the web version of this article.)

a relatively more reducing environment, Thus, moving from the lower right to the upper left, α-Fe_2O_3 (iron as Fe^{3+}) reduces to Fe_3O_4 (iron as $Fe^{2+,3+}$), then reduces to $Fe_{1-x}O$ (iron as Fe^{2+}), and finally Fe metal (iron as Fe^0) is formed.

Superimposed upon Fig. 1 are the conditions where the Biphase surface structure has been reported herein. From this plot it is apparent that the surface structure occurs under conditions where in the bulk α-Fe_2O_3 is being reduced to Fe_3O_4; this is consistent with the current XPS and magnetism results.

A simple model (Fig. 5) to explain the above results is a slab of Fe_3O_4 less than one unit cell thick on the oxygen termination of α-Fe_2O_3. The surface unit cell of the Fe_3O_4 slab is 6.238 Å, the surface unit cell of α-Fe_2O_3 is 5.038 Å (size of the (1 × 1) unit cell), and the cells are rotated 30° in order to preserve the alignment of the similar oxygen sublattices; preservation of oxygen sublattices is a

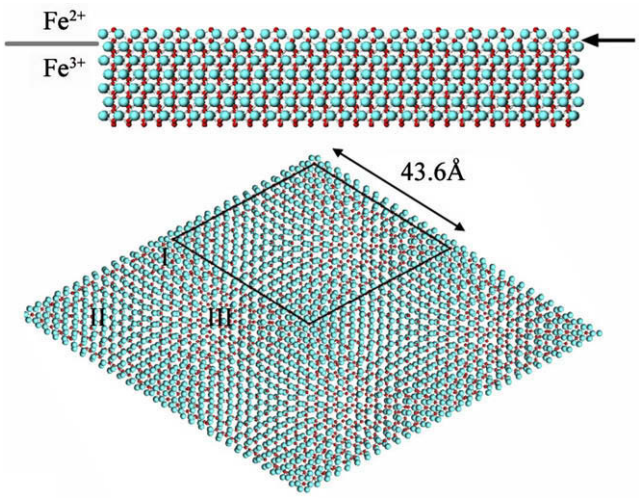

Fig. 5. Model for the Biphase structure. Top: side view. Bottom: plan view showing four of the Biphase unit cells with a 43.6 Å cell marked.

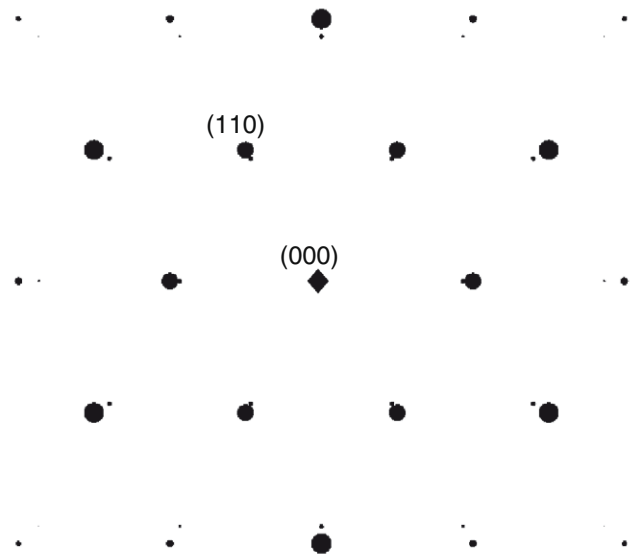

Fig. 6. Simulated kinematical diffraction pattern from the Biphase model, showing both the strong spots (from the bulk) as well as weaker ones (from the surface); this should be compared to Fig. 2. The increasing of distance between the spots here and in Fig. 2 is a characteristic of a simple hex-on-hex configuration, with double-diffraction leading to a fully floreted pattern.

well-known phenomenon in bulk oxides. Placing the Fe_3O_4 slab on α-Fe_2O_3 produces a supercell with a = 43.6 Å, rotated 30° from the α-Fe_2O_3 (1 × 1).

Separate domains of structure within the unit cell can be seen in Fig. 5, consistent with previous STM reports of island-like contrast within a 40 ± 5 Å superlattice cell rotated 30° relative to the α-Fe_2O_3 (1 × 1). Three domains have been marked I, II, and III in Fig. 5. The iron atoms in the surface layer (indicated with an arrow at the top of Fig. 5) are approximately distorted octahedra in domain I, tetrahedra in domain II, and non-standard six-coordinate in domain III. Recall that both α-Fe_2O_3 and $Fe_{1-x}O$ bulk contain only octahedrally coordinated iron cations, and only bulk Fe_3O_4 (and γ-Fe_2O_3) contain tetrahedrally coordinated iron cations. To maintain charge neutrality, the iron atoms in the surface layer are nominally Fe^{2+}. This is consistent with the experimental XPS measurement of the Biphase surface.

A simulated kinematical diffraction pattern for this model is shown in Fig. 6 and strongly resembles the experimentally observed pattern. Note that the florets in the experimental pattern are a result of dynamical scattering and thus are not observed in the kinematical simulation since it only takes into account single scattering events.

5. Discussion

A combination of experimental data with an analysis of the thermodynamic conditions where the Biphase forms as well as a simple model which explains the results has been presented here. The results are consistent with all the published experimental data, and points to the original interpretations of the floreted (LEED) diffraction pattern as resulting from simple double-diffraction as being correct. Perhaps most importantly, the current results are completely consistent with the bulk thermodynamics, which it will be argued they have to be since a surface is always exchanging material with the underlying bulk, albeit slowly. The reduction of α-Fe_2O_3 to Fe_3O_4 in the bulk is a topotactic and crystallographically reversible transformation [49]. Upon nucleation of the Fe_3O_4 slab on the surface of α-Fe_2O_3, growth of the domain can readily occur

into the bulk. That is why domains of Fe_3O_4 are observed to coexist with the so-called Biphase termination and why prolonged annealing in the formation regime lead to a full transformation to Fe_3O_4. According to the model presented here, the only difference between the Biphase and Fe_3O_4 is the thickness of the surface slab (bulk Fe_3O_4 has infinite slab thickness).

The proposed structure herein likely represents a simplified version of the true structure of the so-called Biphase surface. With higher quality diffraction data it is plausible to produce a more accurate model, however the magnetic properties of the sample make this something which cannot be done to the required accuracy using TEM; a better choice might be to use surface X-ray scattering.

6. Summary

The so-called Biphase termination on α-Fe_2O_3 was previously believed to be islands of $Fe_{1-x}O$ and α-Fe_2O_3 arranged in a $\sim$40 Å periodic unit cell based upon a simple interpretation of STM images. This is an inadequate model, and is contradicted by electron diffraction, XPS, and magnetism as well as being in disagreement with the expected bulk thermodynamics. Instead, it is found that the Biphase structure is related to a thin Fe_3O_4-type layer at or near the α-Fe_2O_3 surface, and is a simple hex-on-hex overlayer with double-diffraction leading to the characteristic floreted diffraction pattern that has previously been used as the fingerprint to identify this structure.

Acknowledgments

This work was funded by the DOE under Contract #DE-FG02-03ER15457.

References

[1] P.A. Maurice, M.F. Hochella, G.A. Parks, G. Sposito, U. Schwertmann, Clays and Clay Minerals 43 (1995) 29.
[2] K.R. Reddy, U.S. Parupudi, S.N. Devulapalli, C.Y. Xu, Journal of Hazardous Materials 55 (1997) 135.
[3] H.H. Huang, M.C. Lu, J.N. Chen, Water Research 35 (2001) 2291.
[4] J. Bandara, K. Tennakone, J. Kiwi, Langmuir 17 (2001) 3964.
[5] D.S. Toledano, E.R. Dufresne, V.E. Henrich, Journal of Vacuum Science and Technology A – Vacuum Surfaces and Films 16 (1998) 1050.
[6] D.S. Toledano, V.E. Henrich, Journal of Physical Chemistry B 105 (2001) 3872.
[7] G. Ertl, H. Knözinger, J. Weitkamp, Handbook of Heterogeneous Catalysis, VCH Verlagsgesellschaft mbH, Weinheim, Germany, 1997.
[8] M. Muhler, R. Schlögl, G. Ertl, Journal of Catalysis 138 (1992) 413.
[9] R.J. Lad, V.E. Henrich, Surface Science 193 (1988) 81.
[10] A. Barbieri, W. Weiss, M.A. Vanhove, G.A. Somorjai, Surface Science 302 (1994) 259.
[11] N.G. Condon, F.M. Leibsle, A.R. Lennie, P.W. Murray, D.J. Vaughan, G. Thornton, Physical Review Letters 75 (1995) 1961.
[12] N.G. Condon, F.M. Leibsle, T. Parker, A.R. Lennie, D.J. Vaughan, G. Thornton, Physical Review B 55 (1997) 15885.
[13] N.G. Condon, F.M. Leibsle, A.R. Lennie, P.W. Murray, T.M. Parker, D.J. Vaughan, G. Thornton, Surface Science 397 (1998) 278.
[14] X.G. Wang, W. Weiss, S.K. Shaikhutdinov, M. Ritter, M. Petersen, F. Wagner, R. Schlogl, M. Scheffler, Physical Review Letters 81 (1998) 1038.
[15] G.S. Herman, E.P. McDaniel, S.A. Joyce, Journal of Electron Spectroscopy and Related Phenomena 103 (1999) 433.
[16] S.K. Shaikhutdinov, M. Ritter, X.G. Wang, H. Over, W. Weiss, Physical Review B 60 (1999) 11062.
[17] S.K. Shaikhutdinov, W. Weiss, Surface Science 432 (1999) 627.
[18] G. Ketteler, W. Weiss, W. Ranke, R. Schlogl, Physical Chemistry Chemical Physics 3 (2001) 1114.
[19] N. Camillone, K. Adib, J.P. Fitts, K.T. Rim, G.W. Flynn, S.A. Joyce, R.M. Osgood, Surface Science 511 (2002) 267.
[20] G. Ketteler, W. Ranke, Physical Review B 66 (2002) 3.
[21] U. Leist, W. Ranke, K. Al-Shamery, Physical Chemistry Chemical Physics 5 (2003) 2435.
[22] C.Y. Kim, A.A. Escuadro, M.J. Bedzyk, L. Liu, P.C. Stair, Surface Science 572 (2004) 239.
[23] K.S. Kim, W.E. Baitinger, J.W. Amy, N. Winograd, Journal of Electron Spectroscopy and Related Phenomena 5 (1974) 351.
[24] T.J. Chuang, C.R. Brundle, K. Wandelt, Thin Solid Films 53 (1978) 19.
[25] S. Joshi, P.G. Bilurkar, S.M. Chaudhari, S.M. Kanetkar, S.B. Ogale, Physical Review B 40 (1989) 10635.
[26] A.N. Chiaramonti, P.C. Stair, L.D. Marks, Surface Science 586 (2005) 38.
[27] L. Liu, Methyl Radical Chemistry on Single Crystal Hematite Surfaces and UO_3 Supported on Single Crystal Hematite, Northwestern University, 2005.
[28] W.X. Huang, W. Ranke, R. Schlogl, Journal of Physical Chemistry B 109 (2005) 9202.
[29] W.X. Huang, W. Ranke, R. Schlogl, Journal of Physical Chemistry C 111 (2007) 2198.
[30] T.U. Nahm, W. Kim, S.J. Oh, Journal of the Korean Physical Society 46 (2005) 125.
[31] C. Liu, T.J. Klemmer, N. Shukla, X. Wu, D. Weller, M. Tanase, D. Laughlin, Journal of Magnetism and Magnetic Materials 266 (2003) 96.
[32] R. Dieckmann, H. Schmalzried, Berichte Der Bunsen-Gesellschaft – Physical Chemistry Chemical Physics 81 (1977) 414.
[33] R. Dieckmann, Berichte Der Bunsen-Gesellschaft – Physical Chemistry Chemical Physics 86 (1982) 112.
[34] A.N. Chiaramonti, J.D. Pless, L. Liu, J.P. Smit, C.H. Lanier, K.R. Poeppelmeier, P.C. Stair, L.D. Marks, Crystal Growth and Design 4 (2004) 749.
[35] R. Ai, M.I. Buckett, D. Dunn, T.S. Savage, J.P. Zhang, L.D. Marks, Ultramicroscopy 39 (1991) 387.
[36] C. Collazo-Davila, E. Landree, D. Grozea, G. Jayaram, R. Plass, P.C. Stair, L.D. Marks, Journal of the Microscopy Society of America 1 (1995) 267.
[37] C. Leslie, E. Landree, C. Collazo-Davila, E. Bengu, D. Grozea, L.D. Marks, Microscopy Research and Technique 46 (1999) 160.
[38] L.D. Marks, N. Erdman, A. Subramanian, Journal of Physics – Condensed Matter 13 (2001) 10677.
[39] A. Subramanian, L.D. Marks, Ultramicroscopy 98 (2004) 151.
[40] A.N. Chiaramonti, L.D. Marks, Journal of Materials Research 20 (2005) 1619.
[41] A.N. Chiaramonti, Structure and Thermodynamics of Model Catalytic Oxide Surfaces, Northwestern University, 2005.
[42] C. Lanier, Real and Model Oxide Surfaces, Northwestern University, Evanston, 2007.
[43] P. Hirsch, A. Howie, R.B. Nicholson, D.W. Pashley, M.J. Whelan, Electron Microscopy of Thin Crystals, Krieger Publishing Company, Malabar, Florida, 1977. p. 362.
[44] L.D. Marks, R. Plass, D. Dorset, Surface Review and Letters 4 (1997) 1.
[45] C.R. Brundle, T.J. Chuang, K. Wandelt, Surface Science 68 (1977) 459.
[46] R.A. Robie, B.S. Hemingway, Thermodynamic Properties of Minerals and Related Substances at 298.15 K and 1 Bar (10^5 Pascals) Pressure and at Higher Temperatures, US Geological Survey Bulletin 2131, 1995.
[47] A. Muan, American Journal of Science 256 (1958) 171.
[48] D.E. Miser, E.J. Shin, M.R. Hajaligol, F. Rasouli, Applied Catalysis A: General 258 (2004) 7.
[49] J.J. Heizmann, P. Becker, R. Baro, Journal of Applied Crystallography 14 (1981) 270.
[50] N. Berdunov, S. Murphy, G. Mariotto, I.V. Shvets, Physical Review B 70 (2004) 085404.